ANTsX: A dynamic ecosystem for quantitative biological and medical imaging

Nicholas J. Tustison[1,8], Philip A. Cook[2], Andrew J. Holbrook[3], Hans J. Johnson[4], John Muschelli[5], Gabriel A. Devanyi[6], Jeffrey T. Duda[2], Sandhitsu R. Das[2], Nicholas C. Cullen[7], Daniel L. Gillen[8], Michael A. Yassa[9], James R. Stone[1], James C. Gee[2], Brian B. Avants[1] for the Alzheimer's Disease Neuroimaging Initiative[†]

[1]Department of Radiology and Medical Imaging, University of Virginia, Charlottesville, VA
[2]Department of Radiology, University of Pennsylvania, Philadelphia, PA
[3]Department of Biostatistics, University of California, Los Angeles, CA
[4]Department of Electrical and Computer Engineering, University of Iowa, Philadelphia, PA
[5]School of Public Health, Johns Hopkins University, Baltimore, MD
[6]Douglas Mental Health University Institute, McGill University, Montreal, QC
[7]Lund University, Scania, SE
[8]Department of Statistics, University of California, Irvine, CA
[9]Department of Neurobiology and Behavior, University of California, Irvine, CA

Corresponding authors:
Nicholas J. Tustison, DSc
Department of Radiology and Medical Imaging
University of Virginia
ntustison@virginia.edu

James C. Gee, PhD
Department of Radiology
University of Pennsylvania
gee@upenn.edu

Brian. B. Avants, PhD
Department of Radiology and Medical Imaging
University of Virginia
stnava@gmail.com

[†]Data used in preparation of this article were obtained from the Alzheimer's Disease Neuroimaging Initiative (ADNI) database (http://adni.loni.usc.edu). As such, the investigators within the ADNI contributed to the design and implementation of ADNI and/or provided data but did not participate in analysis or writing of this report. A complete listing of ADNI investigators can be found at: http://adni.loni.usc.edu/wp-content/uploads/how to apply/AD NI Acknowledgement List.pdf

Abstract

The Advanced Normalizations Tools ecosystem, known as ANTsX, consists of multiple open-source software libraries which house top-performing algorithms used worldwide by scientific and research communities for processing and analyzing biological and medical imaging data. The base software library, ANTs, is built upon, and contributes to, the NIH-sponsored Insight Toolkit. Founded in 2008 with the highly regarded Symmetric Normalization image registration framework, the ANTs library has since grown to include additional functionality. Recent enhancements include statistical, visualization, and deep learning capabilities through interfacing with both the R statistical project (ANTsR) and Python (ANTsPy). Additionally, the corresponding deep learning extensions ANTsRNet and ANTsPyNet (built on the popular TensorFlow/Keras libraries) contain several popular network architectures and trained models for specific applications. One such comprehensive application is a deep learning analog for generating cortical thickness data from structural T1-weighted brain MRI. Not only does this significantly improve computational efficiency and provide comparable-to-superior accuracy over the existing ANTs pipeline but it also illustrates the importance of the comprehensive ANTsX approach as a framework for medical image analysis.

The Advanced Noramlization Tools (ANTs) is a state-of-the-art, open-source software toolkit for image registration, segmentation, and other functionality for comprehensive biological and medical image analysis. Historically, ANTs is rooted in advanced image registration techniques which have been at the forefront of the field due to seminal contributions that date back to the original elastic matching method of Bajcsy and co-investigators[1–3] and continues to set the standard in the field. Various independent platforms have been used to evaluate ANTs tools since their early development. In a landmark paper[4], the authors reported an extensive evaluation using multiple neuroimaging datasets analyzed by fourteen different registration tools, including the Symmetric Normalization (SyN) algorithm[5] found in ANTs[6], and found that "ART, SyN, IRTK, and SPM's DARTEL Toolbox gave the best results according to overlap and distance measures, with ART and SyN delivering the most consistently high accuracy across subjects and label sets." This superior performance was reinforced in a completely different pulmonary imaging evaluation, the Evaluation of Methods for Pulmonary Image REgistration 2010 (EMPIRE10)[7], where ANTs was the top performer for the benchmarks used to assess lung registration accuracy and biological plausibility of the inferred transform (i.e., boundary alignment, fissure alignment, landmark correspondence, and displacement field topology). The competition has continued to the present where SyN has remained the top-ranked algorithm. Even indirect assessments have demonstrated the performance superiority of ANTs registration. In the MICCAI 2012 multi-atlas label fusion segmentation challenge for brain data, the joint label fusion algorithm[8] (coupled with SyN) was the top performer. In fact, 6 of the top 10 performing entries in that competition used ANTs for performing the spatial normalization. A separate competition[9] for segmentation of brain tumors from multi-modal MRI held under the auspices of MICCAI 2013 was won by ANTs developers where the registration capabilities were crucial for performance[10]. The following year an ANTs-based entry for the STACOM workshop concerning cardiac motion estimation won the best paper award[11].

The ANTs registration component not only encodes advanced developments in image registration research but also packages these normalization tools as a full-featured platform that includes an extensive library of similarity measures, transformation types, and regularizers

which are built upon the robust Insight Toolkit and vetted by users and developers from all over the world. In fact, based on performance and innovations within the ANTs toolkit and our track record of contributions to the ITK registration development efforts, our group was selected for the most recent major refactoring of the ITK image registration component[12]. Not only did this development involve porting previously reported research but also included several novel contributions. For example, a newly formulated B-spline variant of the original SyN algorithm was proposed and evaluated using multiple publicly available, annotated datasets and demonstrated statistically significant improvement in label overlap measures[13]. Moreover, the ANTs/ITK code is open-source and community-developed which allows the full community, including commercial projects, use and build on this framework.

Since its inception, though, ANTs has expanded significantly beyond its image registration origins. Other core contributions include template building[14], segmentation[15], image preprocessing (e.g., bias correction[16] and denoising[17]), joint label fusion[8,18], and brain cortical thickness estimation[19,20] (cf Table 1). Additionally, ANTs has been integrated into multiple, publicly available workflows such as fMRIprep[21] and the Spinal Cord Toolbox[22]. Frequently used ANTs pipelines, such as cortical thickness estimation[20], have been integrated into Docker containers and packaged as Brain Imaging Data Structure (BIDS)[23] and FlyWheel applications (i.e., "gears"). It has also been independently ported for various platforms including Neurodebian[24] (Debian OS), Neuroconductor[25] (the R statistical project), and Nipype[26] (Python). Even competing softwares, such as FreeSurfer[27], have incorporated well-performing and complementary ANTs components[16,17] into their own libraries.

Over the course of its development, ANTs has been extended to complementary frameworks resulting in the the Python- and R-based ANTsPy and ANTsR toolkits, respectively. These ANTs-based interfaces with extremely popular, high-level, open-source programming platforms have significantly increased the user base of ANTs and facilitated research workflows which were not previously possible. The rapidly rising popularity of deep learning motivated further recent enhancement of ANTs and its extensions. Despite the existence of an abundance of online innovation and code for deep learning algorithms, much of it is disorganized and lacks a uniformity in structure and external data interfaces which would facilitate greater uptake.

Functionality	Citations
SyN registration[5]	2616
bias field correction[16]	2188
ANTs registration evaluation[6]	2013
joint label fusion[18]	669
template generation[14]	423
cortical thickness: implementation[20]	321
MAP-MRF segmentation[15]	319
ITK integration[12]	250
cortical thickness: theory[19]	180

Table 1: The significance of core ANTs tools in terms of their number of citations (from October 17, 2020).

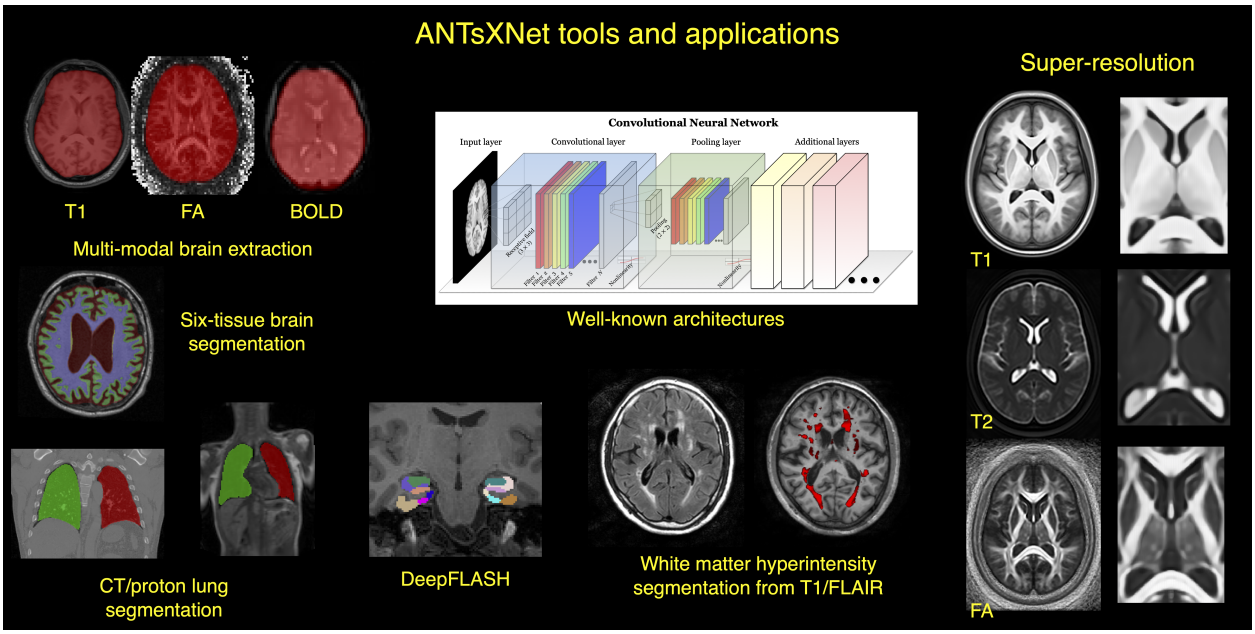

Figure 1: An illustration of the tools and applications available as part of the ANTsRNet and ANTsPyNet deep learning toolkits. Both libraries take advantage of ANTs functionality through their respective language interfaces—ANTsR (R) and ANTsPy (Python). Building on the Keras/TensorFlow language, both libraries standardize popular network architectures within the ANTs ecosystem and are cross-compatible. These networks are used to train models and weights for such applications as brain extraction which are then disseminated to the public.

With this in mind, ANTsR spawned the deep learning ANTsRNet package which is a growing Keras/TensorFlow-based library of popular deep learning architectures and applications specifically geared towards medical imaging. Analogously, ANTsPyNet is an additional ANTsX complement to ANTsPy. Both, which we collectively refer to as "ANTsXNet", are co-developed so as to ensure cross-compatibility such that training performed in one library is readily accessible by the other library. In addition to a variety of popular network architectures (which are implemented in both 2-D and 3-D), ANTsXNet contains a host of functionality for medical image analysis that have been developed in-house and collected from other open-source projects. For example, an extremely popular ANTsXNet application is a multi-modal brain extraction tool that uses different variants of the popular U-net[28] architecture for segmenting the brain in multiple modalities. These modalities include conventional T1-weighted structural MRI as well as T2-weighted MRI, FLAIR, fractional anisotropy and BOLD. Demographic specialization also includes infant T1-weighted and/or T2-weighted MRI. Additionally, we have included other models and weights into our libraries such as a recent BrainAGE estimation model[29], based on $> 14,000$ individuals; HippMapp3r[30], a hippocampal segmentation tool; the winning entry of the MICCAI 2017 white matter hyperintensity segmentation competition[31]; MRI super resolution using deep-projection networks[32]; and NoBrainer, a T1-weighted brain extraction approach based on FreeSurfer. (see Figure 1).

The most recent ANTsX developmental work involves recreating our popular ANTs cortical thickness pipeline[20,33] within the ANTsXNet framework for, amongst other potential benefits, increased computational efficiency. This structural processing pipeline is currently available as open-source within the ANTsXNet libraries which underwent a thorough evaluation using both cross-sectional and longitudinal data and discussed within the context of our previous evaluation of our classical ANTs pipelines[20,33]. Note that related work has been recently reported by external groups[34,35]. Fortunately, these overlapping contributions provide a context for comparison to simultaneously motivate the utility of the ANTsX ecosystem and to editorialize with respect to best practices in the field.

Results

The original ANTs cortical thickness pipeline[20] consists of the following steps:

- preprocessing: denoising[17] and bias correction[36];
- brain extraction[37];
- brain segmentation[15] comprising the
  - cerebrospinal fluid (CSF),
  - gray matter (GM),
  - white matter (WM),
  - deep gray matter,
  - cerebellum, and
  - brain stem; and
- cortical thickness estimation[19].

Our recent longitudinal variant incorporates an additional step involving the construction of a single subject template[14] followed by normal processing.

Although the resulting thickness maps are conducive to voxel-based[38] and related analyses[39], here we employ the well-known Desikan-Killiany-Tourville (DKT)[40] labeling protocol (31 labels per hemisphere) to parcellate the cortex for averaging thickness values regionally. This allows us to 1) be consistent in our evaluation strategy for comparison with our previous work[20,33] and 2) leverage an additional deep learning-based substitution within the proposed pipeline.

Note that the entire analysis/evaluation framework, from preprocessing to statistical analysis, is made possible through the ANTsX ecosystem and simplified through the open-source R and Python platforms. Preprocessing, image registration, and cortical thickness estimation are all available through the ANTsPy and ANTsR libraries whereas the deep learning steps are made possible through networks constructed and trained via ANTsRNet/ANTsPyNet with data augmentation strategies and other utilities built from ANTsR/ANTsPy functionality.

The brain extraction, brain segmentation, and DKT parcellation deep learning components

were trained using data derived from our previous work[20]. Specifically, the IXI[1] , MMRR[41], NKI[2], and OASIS[3] data sets, and the corresponding derived data, comprising over 1200 subjects from age 4 to 94, were used for all network training. Brain extraction employs a traditional 3-D U-net network[28] with whole brain, template-based data augmentation[42] whereas brain segmentation and DKT parcellation are processed via 3-D U-net networks with attention gating[43] on image octant-based batches. We emphasize that a single model was created for each of these steps and was used for all the experiments described below.

Cross-sectional cortical thickness

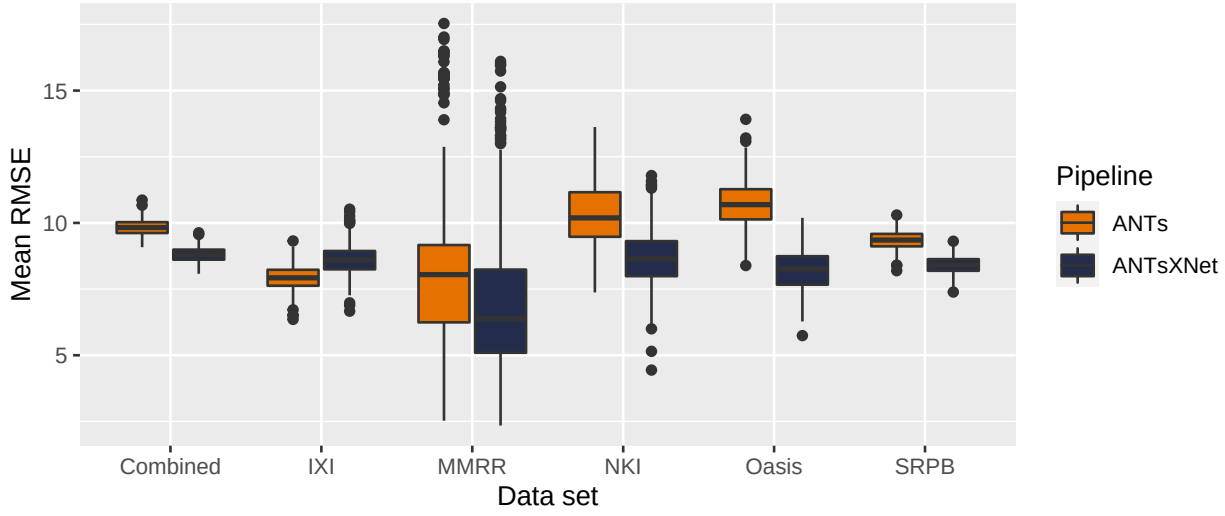

Figure 2: Distribution of mean RMSE values (500 permutations) for age prediction across the different data sets between the traditional ANTs and deep learning-based ANTsXNet pipelines. Total mean values are as follows: Combined—9.3 years (ANTs) and 8.2 years (ANTsXNet); IXI—7.9 years (ANTs) and 8.6 years (ANTsXNet); MMRR—7.9 years (ANTs) and 7.6 years (ANTsXNet); NKI—8.7 years (ANTs) and 7.9 years (ANTsXNet); OASIS—9.2 years (ANTs) and 8.0 years (ANTsXNet); and SRPB—9.2 years (ANTs) and 8.1 years (ANTsXNet).

Due to the absence of ground-truth, we utilize the evaluation strategy from our previous work[20] where we used cross-validation to build and compare age prediction models from data derived from both the proposed ANTsXNet pipeline and the established ANTs pipeline. Specifically, we use "age" as a well-known and widely-available demographic correlate of

[1] https://brain-development.org/ixi-dataset/
[2] http://fcon_1000.projects.nitrc.org/indi/pro/nki.html
[3] https://www.oasis-brains.org

cortical thickness[44] and quantify the predictive capabilities of corresponding random forest classifiers[45] of the form:

$$AGE \sim VOLUME + GENDER + \sum_{i=1}^{62} T(DKT_i) \tag{1}$$

with covariates $GENDER$ and $VOLUME$ (i.e., total intracranial volume).[4] $T(DKT_i)$ is the average thickness value in the i^{th} DKT region. Root mean square error (RMSE) between the actual and predicted ages are the quantity used for comparative evaluation. As we have explained previously[20], we find these evaluation measures to be much more useful than some other commonly applied criteria as they are closer to assessing the actual utility of these thickness measurements as actual biomarkers for disease[46] or growth. For example, in recent work[34] the authors employ correlation with FreeSurfer thickness values as the primary evaluation for assessing relative performance with ANTs cortical thickness[20]. Aside from the fact that this is a prime example of flawed[5] circularity analysis[47], such an evaluation does not indicate relative utility as a biomarker.

In addition to the training data listed above, to ensure generalizability, we also compared performance using the SRPB data set[6] comprising over 1600 participants from 12 sites. Note that we recognize that we are processing data through the proposed deep learning-based pipeline that were used to train certain components of this pipeline. Although this does not provide evidence for generalizability (which is why we include the much larger SRPB data set), it is still interesting to examine the results since, in this case, the deep learning training can be considered a type of noise reduction on the final model. It should be noted that training did not use age prediction (or any other evaluation or related measure) as a criterion to be optimized during network model training (i.e., circular analysis[47]).

[4] We used the randomForest package in R with the default hyperparameter values.

[5] Here, data selection is driven by the same criteria used to evaluate performance. Specifically, DeepSCAN network training utilizes FreeSurfer brain segmentation results. Thickness is highly correlated with segmentation which varies characteristically between relevant software packages. Relative performance with ANTs thickness (which does not use FreeSurfer for training) is then assessed by determining correlations with FreeSurfer thickness values. Almost as problematic is their use of repeatability (which they confusingly label as "robustness") as an additional ranking criterion. Repeatability evaluations should be contextualized within considerations such as the bias-variance tradeoff and quantified using relevant metrics, such as the intra-class correlation coefficient which takes into account both inter- and intra-observer variability.

[6] https://bicr-resource.atr.jp/srpbs1600/

The results are shown in Figure 2 where we used cross-validation with 500 permutations per model per data set (including a "combined" set) and an 80/20 training/testing split. The ANTsXNet deep learning pipeline outperformed the classical pipeline[20] in terms of age prediction in all data sets except for IXI. This also includes the cross-validation iteration where all data sets were combined. Importance plots ranking the cortical thickness regions and the other covariates of Equation (1) are shown in Figure 3. Rankings employ "MeanDecreaseAccuracy" which quantifies the decrease in model accuracy based on the exclusion of that variable. Additionally, repeatability assessment on the MMRR data set yielded ICC values ("average random rater") of 0.99 for both pipelines.

(a) ANTs (b) ANTsXNet

Figure 3: Importance plots for the SRPB data set using "MeanDecreaseAccuracy" for the random forest regressors (i.e., cortical thickness regions, gender, and brain volume specified by Equation (1).

Longitudinal cortical thickness

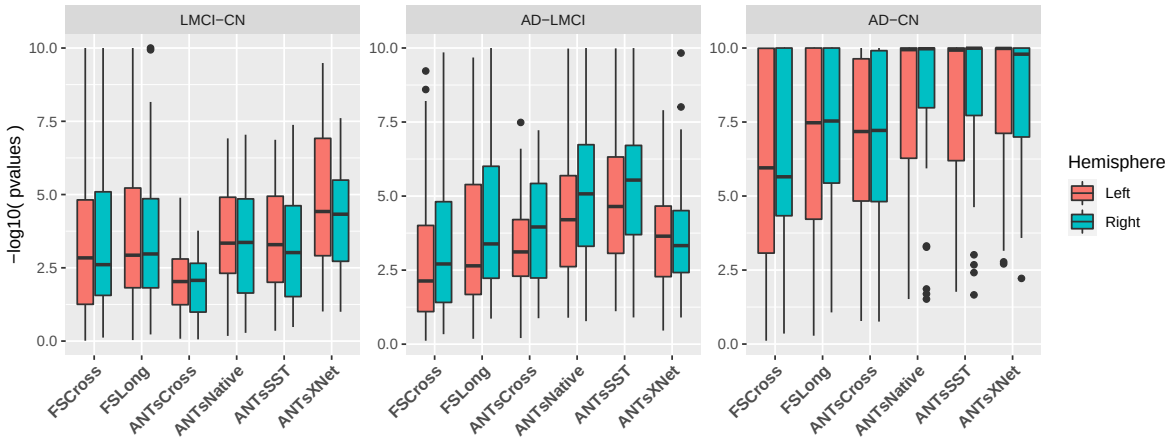

(a)

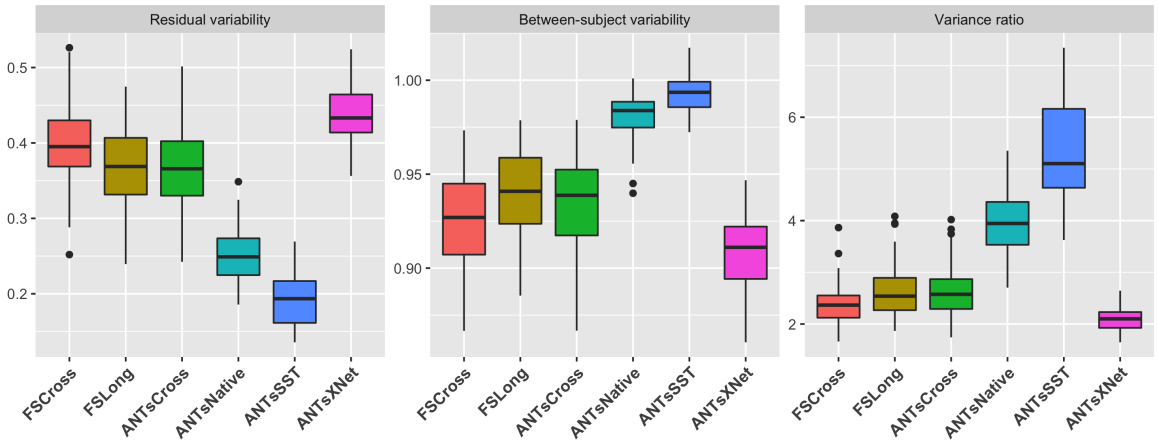

(b)

Figure 4: Measures for the both the supervised and unsupervised evaluation strategies, respectively given in (a) and (b). (a) Log p-values for diagnostic differentiation of LMCI-CN, AD-LMCI, and AD-CN subjects for all pipelines over all DKT regions. (b) Residual variability, between subject, and variance ratio values per pipeline over all DKT regions.

Given the excellent performance and superior computational efficiency of the proposed ANTsXNet pipeline for cross-sectional data, we evaluated its performance on longitudinal data using the longitudinally-specific evaluation strategy and data we employed with the introduction of the longitudinal version of the ANTs cortical thickness pipeline[33]. It should be emphasized that, in contrast to the longitudinal version, the ANTsXNet pipeline is not specifically tailored for longitudinal data, so we regard any positive performance in this domain as a plus that motivates the development of future longitudinal extensions. The

ADNI-1 data used for our previous evaluation[33] consisted of over 600 subjects (197 cognitive normals, 324 LMCI subjects, and 142 AD subjects) with one or more follow-up image acquisition sessions every 6 months (up to 36 months) for a total of over 2500 images. In addition to the ANTsXNet pipeline for the current evaluation, our previous work included the FreeSurfer[27] cross-sectional (FSCross) and longitudinal (FSLong) streams, the ANTs cross-sectional pipeline (ANTsCross) in addition to two longitudinal ANTs-based variants (ANTsNative and ANTsSST). Two evaluation measurements, one unsupervised and one supervised, were used to assess comparative performance between all five pipelines. We add the results of the ANTsXNet pipeline evaluation in relation to these other pipelines to provide a comprehensive overview of relative performance.

The first, supervised evaluation employed Tukey post-hoc analyses with false discovery rate (FDR) adjustment to test the significance of the LMCI-CN, AD-LMCI, and AD-CN diagnostic contrasts. This is provided by the following LME model

$$\begin{aligned}\Delta Y \sim & Y_{bl} + AGE_{bl} + ICV_{bl} + APOE_{bl} + GENDER + DIAGNOSIS_{bl} \\ & + VISIT : DIAGNOSIS_{bl} + (1|ID) + (1|SITE).\end{aligned} \tag{2}$$

Here, ΔY is the change in thickness of the k^{th} DKT region from baseline (bl) thickness Y_{bl} with random intercepts for both the individual subject (ID) and the acquisition site. The subject-specific covariates AGE, $APOE$ status, $GENDER$, $DIAGNOSIS$, and $VISIT$ were taken directly from the ADNIMERGE package.

Second, linear mixed-effects (LME)[48] modeling was used to quantify between-subject and residual variabilities, the ratio of which provides an estimate of the effectiveness of a given biomarker for distinguishing between subpopulations. In order to assess this criteria while accounting for changes that may occur through the passage of time, we used the following

Bayesian LME model:

$$
\begin{aligned}
Y_{ij}^k &\sim N(\alpha_i^k + \beta_i^k t, \sigma_k^2) \\
\alpha_i^k &\sim N(\alpha_0^k, \tau_k^2) \quad \beta_i^k \sim N(\beta_0^k, \rho_k^2) \\
\alpha_0^k, \beta_0^k &\sim N(0, 10) \quad \sigma_k, \tau_k, \rho_k \sim \text{Cauchy}^+(0, 5)
\end{aligned} \tag{3}
$$

where Y_{ij}^k denotes the i^{th} individual's cortical thickness measurement corresponding to the k^{th} region of interest at the time point indexed by j and specification of variance priors to half-Cauchy distributions reflects commonly accepted best practice in the context of hierarchical models[49]. The ratio of interest, r^k, per region of the residual variability, τ_k, and between-subject variability, σ_k is

$$
r^k = \frac{\tau_k}{\sigma_k}, k = 1, \ldots, 62 \tag{4}
$$

where the posterior distribution of r_k was summarized via the posterior median.

Results for both longitudinal evaluation scenarios are shown in Figure 4. Log p-values are provided in Figure 4(a) which demonstrate excellent LMCI-CN and AD-CN differentiation and comparable AD-LMCI diffierentiation relative to the other pipelines. Despite these strong results, Figure 4(b) shows that even better performance may be possible for a longitudinal extension to ANTsXNet. In a longitudinal setting, we prefer to see lower values for residual variability and higher values for between-subject variability, leading to a larger variance ratio. ANTsXNet performs remarkably poorly for these measures, suggesting that even better classification performance—e.g., superior differentiation between LMCI and AD cohorts—is completely possible for an ANTsXNet extension that leverages the longitudinal information the current implementation does not. One such piece of information is repeated measures, i.e., the fact that we observe some subjects multiple times. Failure to account for this information explains lower between-subject variabilities for ANTsXNet. In turn, all variability expresses itself through higher within-subject residuals. But there is an additional reason for ANTsXNet exhibiting higher residual variability. Neural networks achieve their power by increasing their effective degrees of freedom way beyond those of traditional linear models. In terms of the

bias-variance tradeoff, such an increase in model complexity translates to significantly less predictive bias while simultaneously leading to greater predictive variance. This fact explains how ANTsXNet can perform so well while retaining such a large residual variability. An interesting question is how longitudinal extensions to ANTsXNet will perform with respect to the same measure.

Discussion

The ANTsX software ecosystem provides a comprehensive framework for quantitative biological and medical imaging. Although ANTs, the original core of ANTsX, is still at the forefront of image registration technology, it has moved signicantly beyond its image registration origins. This expansion is not confined to technical contributions (of which there are many) but also consists of facilitating access to a wide range of users who can use ANTsX tools (whether through bash scripting, Python scripting or R scripting) to construct tailored pipelines for their own studies or to take advantage of our pre-fabricated pipelines. And given the open-source nature of the ANTsX software, usage is not limited, for example, to academic institutions—a common constraint characteristic of other packages.

One of our most widely used pipelines is the estimation of cortical thickness from neuroimaging. This is understandable given the widespread usage of regional cortical thickness as a biomarker for developmental or pathological trajectories of the brain. In this work, we used this well-vetted ANTs tool to provide training data for producing an alternative version which leverages deep learning for improved computational efficiency and also provides superior performance with respect to previously proposed evaluation measures for both cross-sectional[20] and longitudinal scenarios[33]. In addition to providing the tools which generated the original training data for the proposed ANTsXNet pipeline, the ANTsX ecosystem provides a full-featured platform for the additional steps such as preprocessing (ANTsR/ANTsPy); data augmentation (ANTsR/ANTsPy); network construction and training (ANTsRNet/ANTsPyNet); and visualization and statistical analysis of the results (ANTsR/ANTsPy).

It is the comprehensiveness of ANTsX that provides significant advantages over much of the

deep learning work that is currently taking place in medical imaging and related fields. For example, related work[34] also built a similar pipeline and assessed performance. However, due to the lack of a complete processing and analysis framework, training data was generated using the FreeSurfer stream, deep learning-based brain segmentation employed DeepSCAN[50] (in-house software), and cortical thickness estimation[19] used the ANTs toolkit. For the reader interested in reproducing the authors' results, they are primarily prevented from doing so due, as far as we can tell, to the lack of the public availability of the only software they actually produced themselves, i.e., DeepSCAN. However, even further inhibiting usage is the fact that the external utilities derive from different sources and so issues such as interoperability are relevant.

In terms of future work, the recent surge and utility of deep learning in medical image analysis has significantly guided the areas of active ANTsX development. As demonstrated in this work with our widely used cortical thickness pipeline, there are many potential benefits of deep learning analogs to existing ANTs tools as well as the development of new ones. As mentioned, the proposed cortical thickness pipeline is not specifically tailored for longitudinal data. Nevertheless, performance is comparable-to-superior relative to existing pipelines depending on the evaluation metric. We see possible longitudinal extensions incorporating aspects of the single-subject template construction, as described in our previous work[33], in addition to the possibility of incorporating subject ID and months as additional network inputs.

Methods

Software, average DKT regional thickness values for all data sets, and the scripts to perform both the analysis and obtain thickness values for a single subject are provided as open-source. Specifically, all the ANTsX libraries are hosted on GitHub (https://github.com/ANTsX). The cross-sectional data and analysis code are available as .csv files and R scripts at the GitHub repository dedicated to this paper (https://github.com/ntustison/PaperANTsX) whereas the longitudinal data and evaluation scripts are organized with the repository associated with our previous work[33] (https://github.com/ntustison/CrossLong).

ANTsXNet cortical thickness

```
import ants
import antspynet

# ANTsPy/ANTsPyNet processing for subject IXI002-Guys-0828-T1
t1_file = "IXI002-Guys-0828-T1.nii.gz"
t1 = ants.image_read(t1_file)

# Atropos six-tissue segmentation
atropos = antspynet.deep_atropos(t1, do_preprocessing=True, verbose=True)

# Kelly Kapowski cortical thickness (combine Atropos WM and deep GM)
kk_segmentation = atropos['segmentation_image']
kk_segmentation[kk_segmentation == 4] = 3
kk_gray_matter = atropos['probability_images'][2]
kk_white_matter = atropos['probability_images'][3] + atropos['probability_images'][4]
kk = ants.kelly_kapowski(s=kk_segmentation, g=kk_gray_matter, w=kk_white_matter,
                         its=45, r=0.025, m=1.5, x=0, verbose=1)

# Desikan-Killiany-Tourville labeling
dkt = antspynet.desikan_killiany_tourville_labeling(t1, do_preprocessing=True, verbose=True)

# DKT label propagation throughout the cortex
dkt_cortical_mask = ants.threshold_image(dkt, 1000, 3000, 1, 0)
dkt = dkt_cortical_mask * dkt
kk_mask = ants.threshold_image(kk, 0, 0, 0, 1)
dkt_propagated = ants.iMath(kk_mask, "PropagateLabelsThroughMask", kk_mask * dkt)

# Get average regional thickness values
kk_regional_stats = ants.label_stats(kk, dkt_propagated)
```

Listing 1: ANTsPy/ANTsPyNet command calls for a single IXI subject in the evaluation study.

In Listing 1, we show the ANTsPy/ANTsPyNet code snippet for processing a single subject which starts with reading the T1-weighted MRI input image, through the generation of the Atropos-style six-tissue segmentation and probability images, application of `ants.kelly_kapowski` (i.e., DiReCT), DKT cortical parcellation, subsequent label propagation through the cortex, and, finally, regional cortical thickness tabulation. Computation time on a CPU-only platform is ~1 hour primarily due to the `ants.kelly_kapowski` function. Note that there is a precise, line-by-line R-based analog available through ANTsR/ANTsRNet.

Both the `ants.deep_atropos` and `antspynet.desikan_killiany_tourville_labeling` functions perform brain extraction using the `antspynet.brain_extraction` function. Internally, `antspynet.brain_extraction` contains the requisite code to build the network and assign the appropriate hyperparameters. The model weights are automatically downloaded from the online hosting site https://figshare.com (see the function `get_pretrained_network` in ANTsPyNet or `getPretrainedNetwork` in ANTsRNet for links to all models and weights)

and loaded to the constructed network. `antspynet.brain_extraction` performs a quick translation transformation to a specific template (also downloaded automatically) using the centers of intensity mass, a common alignment initialization strategy. This is to ensure proper gross orientation. Following brain extraction, preprocessing for the other two deep learning components includes `ants.denoise_image` and `ants.n4_bias_correction` and an affine-based reorientation to a version of the MNI template[51]. We recognize the presence of some redundancy due to the repeated application of certain preprocessing steps. Thus, each function has a `do_preprocessing` option to eliminate this redundancy for knowledgeable users but, for simplicity in presentation purposes, we do not provide this modified pipeline here. Although it should be noted that the time difference is minimal considering the longer time required by `ants.kelly_kapowski`. `ants.deep_atropos` returns the segmentation image as well as the posterior probability maps for each tissue type listed previously. `antspynet.desikan_killiany_tourville_labeling` returns only the segmentation label image which includes not only the 62 cortical labels but the remaining labels as well. The label numbers and corresponding structure names are given in the program help. Because the DKT parcellation will, in general, not exactly coincide with the non-zero voxels of the resulting cortical thickness maps, we perform a label propagation step to ensure the entire cortex, and only the non-zero thickness values in the cortex, are included in the tabulated regional values.

Training

Training differed slightly between models and so we provide details for each of these components below. For all training, we used ANTsRNet scripts and custom batch generators. Although the network construction and other functionality is available in both ANTsPyNet and ANTsRNet (as is model weights compatibility), we have not written such custom batch generators for the former (although this is on our to-do list). In terms of hardware, all training was done on a DGX (GPUs: 4X Tesla V100, system memory: 256 GB LRDIMM DDR4).

T1-weighted brain extraction. A whole-image 3-D U-net model[28] was used in conjunction

with multiple training sessions employing a Dice loss function followed by categorical cross entropy. As mentioned previously, a center-of-mass-based transformation to a standard template was used to standardize such parameters as orientation and voxel size. However, to account for possible different header orientations of input data, a template-based data augmentation scheme was used[42] whereby forward and inverse transforms are used to randomly warp batch images between members of the training population (followed by reorientation to the standard template). A digital random coin flipping for possible histogram matching[52] between source and target images further increased possible data augmentation. Although not detailed here, training for brain extraction in other modalities was performed similarly.

Deep Atropos. Dealing with 3-D data presents unique barriers for training that are often unique to medical imaging. Various strategies are employed such as minimizing the number of layers and/or the number of filters at the base layer of the U-net architecture (as we do for brian extraction). However, we found this to be too limiting for capturing certain brain structures such as the cortex. 2-D and 2.5-D approaches are often used with varying levels of success but we also found better performance using full 3-D information. This led us to try randomly selected 3-D patches of various sizes. However, for both the six-tissue segmentations and DKT parcellations, we found that an octant-based patch strategy yielded the desired results. Specifically, after a brain extracted affine normalization to the MNI template, the normalized image is cropped to a size of [160, 190, 160]. Overlapping octant patches of size [112, 112, 112] were extracted from each image and trained using a batch size of 12 such octant patches with weighted categorical cross entropy as the loss function. As we point out in our earlier work[20], obtaining proper brain segmentation is perhaps the most critical step to estimating thickness values that have the greatest utility as a potential biomarker. In fact, the first and last authors (NT and BA, respectively) spent much time during the original ANTs pipeline development[20] trying to get the segmentation correct which required manually looking at many images and manually adjusting where necessary. This fine-tuning is often omitted or not considered when other groups[34,53,54] use components of our cortical thickness pipeline which can be potentially problematic[55]. Fine-tuning for this particular workflow was also performed between the first and last authors

using manual variation of the weights in the weighted categorical cross entropy. Ultimately, we settled on a weight vector of $(0.05, 1.5, 1, 3, 4, 3, 3)$ for the CSF, GM, WM, Deep GM, brain stem, and cerebellum, respectively. Other hyperparameters can be directly inferred from explicit specification in the actual code. As mentioned previously, training data was derived from application of the ANTs Atropos segmentation[15] during the course of our previous work[20]. Data augmentation included small affine and deformable perturbations using `antspynet.randomly_transform_image_data` and random contralateral flips.

Desikan-Killiany-Tourville parcellation. Preprocessing for the DKT parcellation training was similar to the Deep Atropos training. However, the number of labels and the complexity of the parcellation required deviation from other training steps. First, labeling was split into an inner set and an outer set. Subsequent training was performed separately for both of these sets. For the cortical labels, a set of corresponding input prior probability maps were constructed from the training data (and are also available and automatically downloaded, when needed, from https://figshare.com). Training occurred over multiple sessions where, initially, categorical cross entropy was used and then subsquently refined using a Dice loss function. Whole-brain training was performed on a brain-cropped template size of [96, 112, 96]. Inner label training was performed similarly to our brain extraction training where the number of layers at the base layer was reduced to eight. Training also occurred over multiple sessions where, initially, categorical cross entropy was used and then subsquently refined using a Dice loss function. Other hyperparameters can be directly inferred from explicit specification in the actual code. Training data was derived from application of joint label fusion[18] during the course of our previous work[20]. When calling `antspynet.desikan_killiany_tourville_labeling`, inner labels are estimated first followed by the outer, cortical labels.

References

1. Bajcsy, R. & Broit, C. Matching of deformed images. in *Sixth International Conference on Pattern Recognition (ICPR'82)* 351–353 (1982).

2. Bajcsy, R. & Kovacic, S. Multiresolution elastic matching. *Computer Vision, Graphics, and Image Processing* **46**, 1–21 (1989).

3. Gee, J., Sundaram, T., Hasegawa, I., Uematsu, H. & Hatabu, H. Characterization of regional pulmonary mechanics from serial magnetic resonance imaging data. *Acad Radiol* **10**, 1147–52 (2003).

4. Klein, A. *et al.* Evaluation of 14 nonlinear deformation algorithms applied to human brain MRI registration. *Neuroimage* **46**, 786–802 (2009).

5. Avants, B. B., Epstein, C. L., Grossman, M. & Gee, J. C. Symmetric diffeomorphic image registration with cross-correlation: Evaluating automated labeling of elderly and neurodegenerative brain. *Med Image Anal* **12**, 26–41 (2008).

6. Avants, B. B. *et al.* A reproducible evaluation of ANTs similarity metric performance in brain image registration. *Neuroimage* **54**, 2033–44 (2011).

7. Murphy, K. *et al.* Evaluation of registration methods on thoracic CT: The EMPIRE10 challenge. *IEEE Trans Med Imaging* **30**, 1901–20 (2011).

8. Wang, H. *et al.* Multi-atlas segmentation with joint label fusion. *IEEE Trans Pattern Anal Mach Intell* **35**, 611–23 (2013).

9. Menze, B., Reyes, M. & Van Leemput, K. The multimodal brain tumor image segmentation benchmark (BRATS). *IEEE Trans Med Imaging* (2014) doi:10.1109/TMI.2014.2377694.

10. Tustison, N. J. *et al.* Optimal symmetric multimodal templates and concatenated random forests for supervised brain tumor segmentation (simplified) with *ANTsR*. *Neuroinformatics* (2014) doi:10.1007/s12021-014-9245-2.

11. Tustison, N. J., Yang, Y. & Salerno, M. Advanced normalization tools for cardiac motion correction. in *Statistical atlases and computational models of the heart - imaging and modelling challenges* (eds. Camara, O. et al.) vol. 8896 3–12 (Springer International Publishing, 2015).

12. Avants, B. B. *et al.* The Insight ToolKit image registration framework. *Front Neuroinform* **8**, 44 (2014).

13. Tustison, N. J. & Avants, B. B. Explicit B-spline regularization in diffeomorphic image registration. *Front Neuroinform* **7**, 39 (2013).

14. Avants, B. B. *et al.* The optimal template effect in hippocampus studies of diseased populations. *Neuroimage* **49**, 2457–66 (2010).

15. Avants, B. B., Tustison, N. J., Wu, J., Cook, P. A. & Gee, J. C. An open source multivariate framework for n-tissue segmentation with evaluation on public data. *Neuroinformatics* **9**, 381–400 (2011).

16. Tustison, N. J. & Gee, J. C. N4ITK: Nick's N3 ITK implementation for MRI bias field correction. *The Insight Journal* (2009).

17. Manjón, J. V., Coupé, P., Martí-Bonmatí, L., Collins, D. L. & Robles, M. Adaptive non-local means denoising of MR images with spatially varying noise levels. *J Magn Reson Imaging* **31**, 192–203 (2010).

18. Wang, H. & Yushkevich, P. A. Multi-atlas segmentation with joint label fusion and corrective learning-an open source implementation. *Front Neuroinform* **7**, 27 (2013).

19. Das, S. R., Avants, B. B., Grossman, M. & Gee, J. C. Registration based cortical thickness measurement. *Neuroimage* **45**, 867–79 (2009).

20. Tustison, N. J. *et al.* Large-scale evaluation of ANTs and FreeSurfer cortical thickness measurements. *Neuroimage* **99**, 166–79 (2014).

21. Esteban, O. *et al.* FMRIPrep: A robust preprocessing pipeline for functional mri. *Nat*

Methods **16**, 111–116 (2019).

22. De Leener, B. *et al.* SCT: Spinal cord toolbox, an open-source software for processing spinal cord MRI data. *Neuroimage* **145**, 24–43 (2017).

23. Gorgolewski, K. J. *et al.* The brain imaging data structure, a format for organizing and describing outputs of neuroimaging experiments. *Sci Data* **3**, 160044 (2016).

24. Halchenko, Y. O. & Hanke, M. Open is not enough. Let's take the next step: An integrated, community-driven computing platform for neuroscience. *Front Neuroinform* **6**, 22 (2012).

25. Muschelli, J. *et al.* Neuroconductor: An R platform for medical imaging analysis. *Biostatistics* **20**, 218–239 (2019).

26. Gorgolewski, K. *et al.* Nipype: A flexible, lightweight and extensible neuroimaging data processing framework in python. *Front Neuroinform* **5**, 13 (2011).

27. Fischl, B. FreeSurfer. *Neuroimage* **62**, 774–81 (2012).

28. Falk, T. *et al.* U-net: Deep learning for cell counting, detection, and morphometry. *Nat Methods* **16**, 67–70 (2019).

29. Bashyam, V. M. *et al.* MRI signatures of brain age and disease over the lifespan based on a deep brain network and 14,468 individuals worldwide. *Brain* **143**, 2312–2324 (2020).

30. Goubran, M. *et al.* Hippocampal segmentation for brains with extensive atrophy using three-dimensional convolutional neural networks. *Hum Brain Mapp* **41**, 291–308 (2020).

31. Li, H. *et al.* Fully convolutional network ensembles for white matter hyperintensities segmentation in mr images. *Neuroimage* **183**, 650–665 (2018).

32. Haris, M., Shakhnarovich, G. & Ukita, N. Deep back-projection networks for super-resolution. in *2018 IEEE/CVF Conference on Computer Vision and Pattern Recognition* 1664–1673 (2018). doi:10.1109/CVPR.2018.00179.

33. Tustison, N. J. *et al.* Longitudinal mapping of cortical thickness measurements: An Alzheimer's Disease Neuroimaging Initiative-based evaluation study. *J Alzheimers Dis* (2019) doi:10.3233/JAD-190283.

34. Rebsamen, M., Rummel, C., Reyes, M., Wiest, R. & McKinley, R. Direct cortical thickness estimation using deep learning-based anatomy segmentation and cortex parcellation. *Hum Brain Mapp* (2020) doi:10.1002/hbm.25159.

35. Henschel, L. *et al.* FastSurfer - a fast and accurate deep learning based neuroimaging pipeline. *Neuroimage* **219**, 117012 (2020).

36. Tustison, N. J. *et al.* N4ITK: Improved N3 bias correction. *IEEE Trans Med Imaging* **29**, 1310–20 (2010).

37. Avants, B. B., Klein, A., Tustison, N. J., Woo, J. & Gee, J. C. Evaluation of open-access, automated brain extraction methods on multi-site multi-disorder data. in *16th annual meeting for the organization of human brain mapping* (2010).

38. Ashburner, J. & Friston, K. J. Voxel-based morphometry–the methods. *Neuroimage* **11**, 805–21 (2000).

39. Avants, B. *et al.* Eigenanatomy improves detection power for longitudinal cortical change. *Med Image Comput Comput Assist Interv* **15**, 206–13 (2012).

40. Klein, A. & Tourville, J. 101 labeled brain images and a consistent human cortical labeling protocol. *Front Neurosci* **6**, 171 (2012).

41. Landman, B. A. *et al.* Multi-parametric neuroimaging reproducibility: A 3-T resource study. *Neuroimage* **54**, 2854–66 (2011).

42. Tustison, N. J. *et al.* Convolutional neural networks with template-based data augmentation for functional lung image quantification. *Acad Radiol* **26**, 412–423 (2019).

43. Schlemper, J. *et al.* Attention gated networks: Learning to leverage salient regions in medical images. *Med Image Anal* **53**, 197–207 (2019).

44. Lemaitre, H. *et al.* Normal age-related brain morphometric changes: Nonuniformity across cortical thickness, surface area and gray matter volume? *Neurobiol Aging* **33**, 617.e1–9 (2012).

45. Breiman, L. Random forests. *Machine Learning* **45**, 5–32 (2001).

46. Holbrook, A. J. *et al.* Anterolateral entorhinal cortex thickness as a new biomarker for early detection of Alzheimer's disease. *Alzheimer's & Dementia: Diagnosis, Assessment & Disease Monitoring* **12**, e12068 (2020).

47. Kriegeskorte, N., Simmons, W. K., Bellgowan, P. S. F. & Baker, C. I. Circular analysis in systems neuroscience: The dangers of double dipping. *Nat Neurosci* **12**, 535–40 (2009).

48. Verbeke, G. Linear mixed models for longitudinal data. in *Linear mixed models in practice* 63–153 (Springer, 1997).

49. Gelman, A. & others. Prior distributions for variance parameters in hierarchical models (comment on article by Browne and Draper). *Bayesian analysis* **1**, 515–534 (2006).

50. McKinley, R. *et al.* Few-shot brain segmentation from weakly labeled data with deep heteroscedastic multi-task networks. *CoRR* **abs/1904.02436**, (2019).

51. Fonov, V. S., Evans, A. C., McKinstry, R. C., Almli, C. & Collins, D. L. Unbiased nonlinear average age-appropriate brain templates from birth to adulthood. *NeuroImage* **S102**, (2009).

52. Nyúl, L. G. & Udupa, J. K. On standardizing the MR image intensity scale. *Magn Reson Med* **42**, 1072–81 (1999).

53. Clarkson, M. J. *et al.* A comparison of voxel and surface based cortical thickness estimation methods. *Neuroimage* **57**, 856–65 (2011).

54. Schwarz, C. G. *et al.* A large-scale comparison of cortical thickness and volume methods for measuring alzheimer's disease severity. *Neuroimage Clin* **11**, 802–812 (2016).

55. Tustison, N. J. *et al.* Instrumentation bias in the use and evaluation of scientific software: Recommendations for reproducible practices in the computational sciences. *Front Neurosci* **7**, 162 (2013).